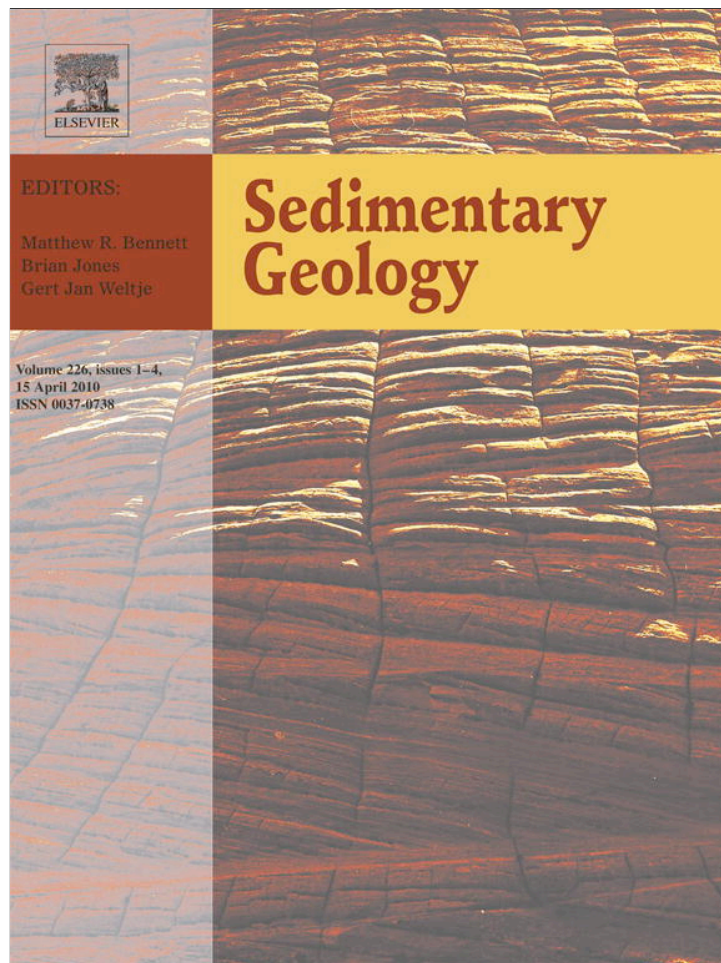


Provided for non-commercial research and education use.
Not for reproduction, distribution or commercial use.



This article appeared in a journal published by Elsevier. The attached copy is furnished to the author for internal non-commercial research and education use, including for instruction at the authors institution and sharing with colleagues.

Other uses, including reproduction and distribution, or selling or licensing copies, or posting to personal, institutional or third party websites are prohibited.

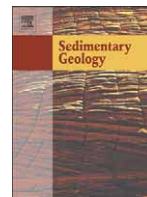
In most cases authors are permitted to post their version of the article (e.g. in Word or Tex form) to their personal website or institutional repository. Authors requiring further information regarding Elsevier's archiving and manuscript policies are encouraged to visit:

<http://www.elsevier.com/copyright>



Contents lists available at ScienceDirect

Sedimentary Geology

journal homepage: www.elsevier.com/locate/sedgeo

Paleoceanographic constraints on Precambrian phosphorite accumulation, Baraga Group, Michigan, USA

Gabriel J. Nelson^{a,1}, Peir K. Pufahl^{a,*}, Eric E. Hiatt^b

^a Department of Earth and Environmental Science, Acadia University Wolfville, Nova Scotia, Canada B4P 2R6

^b Department of Geology, University of Wisconsin-Oshkosh Oshkosh, Wisconsin, 54901, USA

ARTICLE INFO

Article history:

Received 15 November 2009

Received in revised form 9 February 2010

Accepted 10 February 2010

Available online 20 February 2010

Communicated by B. Jones

Keywords:

Precambrian

Phosphorites

Michigan

Baraga Group

Sedimentology

Oceanography

ABSTRACT

The Palaeoproterozoic Baraga Group (ca. 1850 ± 1 Ma) of northern Michigan is a ~1200 m thick sedimentary succession of marine clastic, iron formation, chert, and phosphatic sedimentary rocks that accumulated at the peak of the world's first major phosphogenic episode. Lithofacies stacking patterns are interpreted to record the flooding of the Nuna continental margin during two sea-level cycles. The base of the first sequence is marked by a transgressive lag on Archean basement that is transitional into a highstand accumulation of sandstones deposited in peritidal environments. The bottom of the second sequence is characterized by a chert and carbonate unit with numerous subaerial exposure surfaces deposited in intertidal to supratidal environments. This chert grades upward into subtidal deposits composed of interbedded organic-rich mudstone and sandstone. The highstand and falling stage systems tracts are composed of progradational deltaic deposits. Sequences were framed using the newly discovered Sudbury impact ejecta horizon as a datum. Its emplacement approximately coincides with unrelated environmental changes that increased the delivery of river-borne sediment to the Nuna margin.

Iron bearing minerals ankerite, siderite, and pyrite show that ferrous iron was present in peritidal to deep marine environments. Ankerite dominates nearshore settings where pyrite is absent; pyrite occurs in deeper, progradational deltaic deposits where sulfide was produced by bacterial sulfate reduction. Phosphorite is restricted to shallow-water sediments of the first sequence and the lowstand of the second sequence. Precipitation is interpreted to be the result of Fe-redox pumping just below the sediment–water interface where photosynthetically-produced, nearshore oxygen oases impinged on the seafloor. Such shallow-water phosphorite accumulation is in stark contrast to many Phanerozoic depositional systems in which phosphogenesis occurs across the shelf. This difference likely reflects the dissimilarity in the oxygenation state of the seafloor. In the Precambrian, Fe-redox pumping and thus, phosphogenesis, was restricted to shallow-water settings with a suboxic seafloor. In the Phanerozoic, phosphorite forms in the full spectrum of shelf environments because the entire seafloor is generally well oxygenated. The concentration of bioavailable P in neritic environments during the Proterozoic may have played a major role in the development of benthic microbial ecosystems and evolving eukaryotes.

© 2010 Elsevier B.V. All rights reserved.

1. Introduction

Phosphorite is a marine bio-chemical sedimentary rock generally associated with coastal upwelling (e.g. Glenn et al., 1994; Pufahl, *in press*). Apart from being the primary source of P for fertilizer manufacture, it is also the most important long-term sink in the global P cycle. In Phanerozoic coastal upwelling environments P is extracted from the surface ocean by phytoplankton and authigenically converted to carbonate fluorapatite in the accumulating organic-rich mud below (Glenn et al., 1994). In the Phanerozoic this process governs primary productivity (Filippelli and Delaney, 1994), and

ultimately controls the rate at which carbon dioxide is removed from the atmosphere and deposited as sedimentary organic matter (Föllmi et al., 1993). The accumulation of organic-rich, phosphatic strata is thus, an important feedback that regulates climate.

Although the processes of Phanerozoic phosphorite accumulation are generally well understood, the environmental conditions and feedbacks that produced Precambrian phosphorite remain largely unresolved. This is due in part to the abundance and economic importance of Phanerozoic deposits as well as the scarcity of Precambrian phosphatic sedimentary rocks (Cook and Shergold, 1986). Thus, few studies exist that document Precambrian phosphorite (e.g. Melezhik et al., 2005), attributes of which reflect the biogeochemical cycling of P on the early Earth.

This paper focuses on especially well preserved Precambrian phosphorite in the Palaeoproterozoic Baraga Group (ca. 1850 ± 1 Ma)

* Corresponding author.

E-mail address: peir.pufahl@acadiau.ca (P.K. Pufahl).

¹ Current address: Geoscience Australia, Canberra, ACAT, 2601, Australia.

of northern Michigan (Fig. 1). The Baraga Group is composed of terrigenous clastic, peritidal, shallow shelf, deltaic and chemical sedimentary rocks (Nelson, 2008) that accumulated near the end of the Earth's first phosphogenic episode (Kholodov and Butuzova, 2001; Pufahl, in press). The physical-chemical conditions that produced phosphorite in the Baraga Group and therefore within this initial phosphogenic event, are determined by reconstructing paleoenvironments of deposition and relating variability in phosphatic lithofacies to authigenic and physical sedimentary processes.

Because the accumulation of the Baraga Group also coincides with the onset of sulfidic ocean conditions (Canfield, 1998; Poulton et al., 2004; Johnston et al., 2006) such information may also provide new insight into the composition and structure of the ocean during this event. The transition to a sulfidic ocean is regarded as one of the most significant changes in seawater chemistry in Earth history. It is interpreted to have ended widespread iron formation deposition (Canfield, 1998; Poulton et al., 2004) as well as contributed to a long lull in the evolution of eukaryotes (Anbar and Knoll, 2002; Johnston et al., 2009). The apparent coincidence of the sulfidic ocean transition and deposition of phosphorite in the Baraga Group (Kholodov and Butuzova, 2001; Pufahl, in press) provides a unique opportunity to determine whether the demise of Palaeoproterozoic iron formation and phosphorite are related.

2. Geologic setting

Deposition of the Baraga Group occurred in the Baraga Basin, which is a sub-basin of the larger Animikie Basin (Fig. 1). Sedimentologic and geochemical data suggest that the Animikie Basin evolved from a back-arc (Hemming et al., 1995; Van Wyck and Johnson, 1997) to a foreland basin (Hoffman, 1987; Morey and Southwick, 1995; Ojakangas et al., 2001; Johnston et al., 2006) during the Penokean orogen (Van Wyck and Johnson, 1997; Schneider et al., 2002). Back-

arc deposits consist of Superior-type iron formation and alkaline volcanics whereas deltaic deposits dominate the foreland fill. The emplacement of the newly discovered Sudbury ejecta horizon is approximately coincident with the transition from a back-arc to foreland setting.

The Penokean orogen is one of many circum-Nuna, Palaeoproterozoic orogenies and records the accretion of an island arc, the Wisconsin Magmatic Terrane, to the southern Superior Province (Van Wyck and Johnson, 1997). Accretion is interpreted to have begun ca 1.88 Ga, progressed from the southeast to the northwest, and was complete by ca. 1.84 Ga (Schneider et al., 2002). The boundary between the Wisconsin Magmatic Terrane and the Superior Province is the Niagara Fault Zone, a regional 10 km-wide ductile shear zone (Schneider et al., 2002). North of the Niagara Fault Zone is the Great Lake Tectonic Zone (Fig. 1), an Archean crustal suture that can be traced across northern Michigan and central Minnesota. The Great Lake Tectonic Zone was reactivated during the Penokean orogen and divides the stable craton in the north from the more mobile deformed zone in the south (Ojakangas, 1994). Bisecting the Animikie Basin are the volcanic, sedimentary, and plutonic rocks of the Midcontinent Rift System. These rocks range in age from ca. 1.15 to 1.10 Ga and are interpreted to record incomplete rifting of the Superior Province (Heaman et al., 2007).

The Baraga Group consists of ~1200 m of molasse that accumulated during the Penokean orogen (Schneider et al., 2002), the latter stages of which metamorphosed this succession to greenschist facies (Ojakangas et al., 2001). The Baraga Group forms the upper part of the Marquette Range Supergroup (Ojakangas et al., 2001) and is composed primarily of prograding delta complexes and deeper water hemipelagites. Phosphatic sedimentary rocks are generally associated with peritidal iron formation that was deposited along clastic-starved segments of the coastline. An age of ca. 1850 ± 1 Ma for the Baraga Group is obtained from an interbedded meteorite ejecta

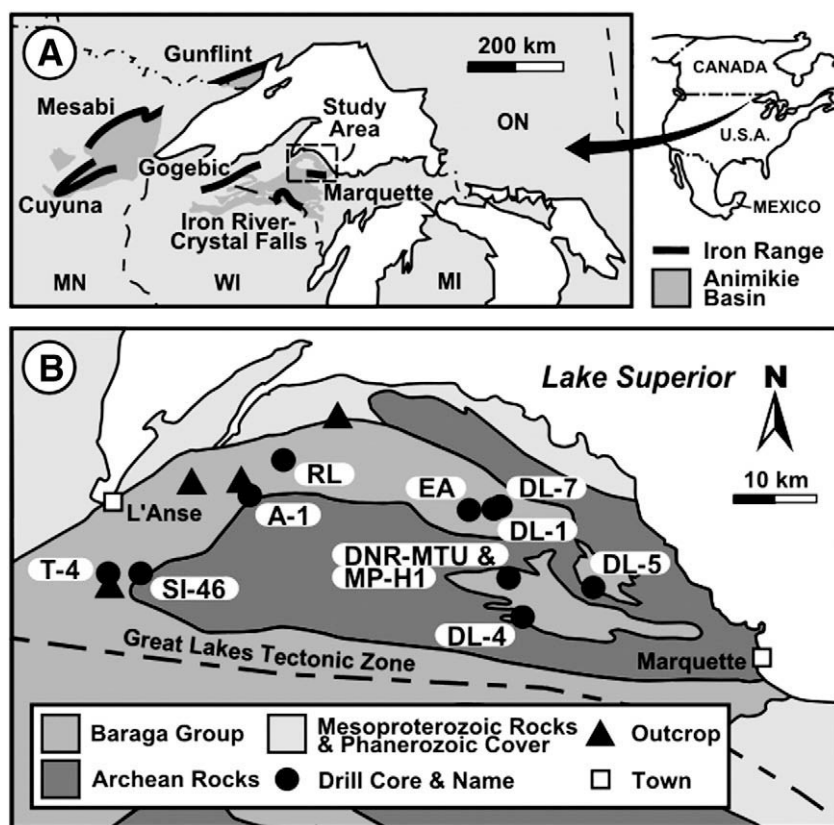


Fig. 1. A) Lake Superior Region of North America showing iron ranges (black) and present extent of Animikie Basin sedimentary rocks. B) Study area with drill core and outcrop locations.

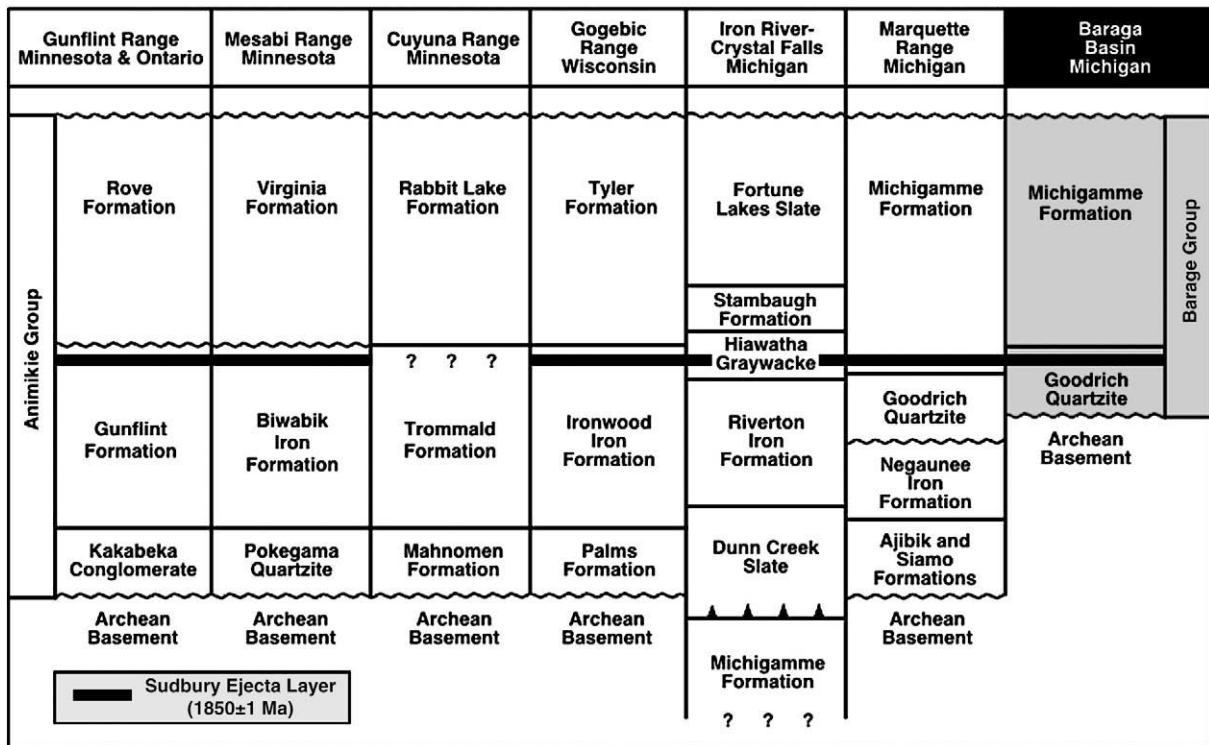


Fig. 2. Correlation of Baraga Group to stratigraphically equivalent strata in the Lake Superior Region. Modified from Cannon et al. (2009).

layer interpreted to have been produced by the Palaeoproterozoic Sudbury impact event (Pufahl et al., 2007; Cannon et al., 2009).

3. Baraga Group stratigraphy

The stratigraphic position of the Sudbury ejecta layer (Addison et al., 2005; Pufahl et al., 2007) confirms that the Baraga Group is equivalent to the Rove and Virginia formations of the Animikie Group in Ontario and Minnesota, respectively (Fig. 2; Ojakangas et al., 2001). Throughout much of northern Michigan the Baraga Group has been eroded so that rocks of the Mid-continental Rift System or unconsolidated sediment lie directly at surface. It consists of the Goodrich Quartzite, a fluvial to tidally deposited basal sandstone, and the Michiganme Formation, a terrigenous clastic unit of interbedded deltaic sandstone, organic-rich siltstone, and iron formation (Fig. 3; Ojakangas et al., 2001). The Michiganme Formation has been subdivided into a lower shaly member, which is also interpreted to have accumulated in a tide-dominated environment, and an upper

sandy member inferred to consist primarily of deltaic deposits. A third member, the Bijiki Iron Formation, is not as laterally persistent; when present it is generally well laminated and conformably overlies the shales of the lower member, suggesting deposition below wave base (Ojakangas, 1994). Phosphorite is restricted to the lower Michiganme Formation (Bijiki Iron Formation and lower Michiganme members; Mancuso et al., 1975; Cannon and Klasner, 1976; Hall, 1985).

4. Methods

Because the Baraga Group is limited in outcrop exposure, drill cores were selected to provide both vertical and lateral stratigraphic context of sedimentologic units. Emphasis was placed on understanding paleoenvironments, regional stratigraphic trends, and collection of samples for petrographic analysis. Interpretations are based on bed-by-bed description and sampling of 16 continuously cored drill holes. A total of 5024 m of drill core was logged that dissects a host of strandline and hemipelagic environments across the Animikie shelf. Paleocurrent measurements were obtained from three oriented drill cores.

Percentages of chemical sedimentary and terrigenous silt- and sand-sized grains were estimated from 132 thin sections and were given an abundance index of rare (1–5% of particles), uncommon (6–30% of particles), common (31–60% of particles), or abundant (>60% particles). Phosphatic crusts and grains were examined in carbon-coated thin sections using secondary and back-scattered electron imaging on a JEOL JSM-5900LV scanning electron microscope equipped with a quantitative Princeton Gamma-Tech IMIX-PC EDS system. Mineral identification was aided by using standard X-ray powder diffraction. Back-loaded, powdered samples from 15 hand specimens were analyzed on an XpertPro Philips powder diffractometer across scattering angles from 5° to 70° using a cobalt X-ray target source. Because sedimentary apatite often contains low concentrations of Th and U, a Radiometric Systems GR-135G hand-held gamma-ray spectrometer was used in the field to assist in identifying phosphatic intervals for sampling.

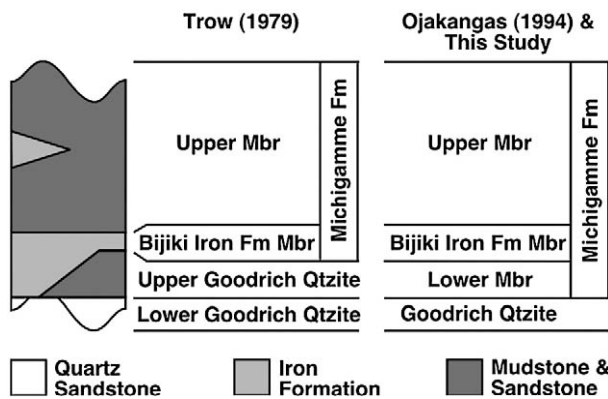


Fig. 3. Comparison of stratigraphic terminology used in this paper to previous schemes (Trow, 1979; Ojakangas, 1994).

5. Depositional framework and sequence stratigraphy

The Baraga Group can be subdivided into nine lithofacies (Table 1): six terrigenous clastic and three chemical. Lithofacies are interpreted to have accumulated in an array of strandline, subtidal, and hemipelagic environments along the Nuna continental margin through two relative sea-level cycles (Fig. 4). Interpretation was aided by correlating the 1850 ± 1 Ma Sudbury impact layer across the Baraga Basin. Systems tracts were interpreted using criteria established by [Plint and Nummedal \(2000\)](#).

5.1. Sequence 1

The first sequence is 8 to 86 m thick and records deposition of the Goodrich Quartzite (Fig. 4). Its base is marked by a transgressive lag that mantles the Archean basement. This pebble conglomerate may represent the transition from tidally influenced fluvial systems to shallow subtidal conditions. Facies F1 is locally arkosic and thickens dramatically in some sections, and probably represents in filling of paleotopography on the underlying Archean basement. Transgression led to deposition of high-energy shoreline deposits (F1) that are in turn overlain by tidal sediments of the highstand systems tract (F2). The falling stage systems tract is composed of progradational tidal flat sediments (F2) of the lower Michigamme Formation. Paleocurrents

from cross-bedded and rippled sandstones (F1 and F2) indicate that tidal currents radiated away from a basement high in the centre of the Baraga Basin ([Ojakangas, 1994](#)).

5.1.1. Transgressive systems tract

Lowstand deposits of the first sequence do not occur in the Baraga Basin, but are present west and north in deeper areas of the Animikie Basin. The transgressive systems tract (TST) ranges from 3 to 47 m in thickness and is preserved in six drill cores, SI-46, A-1, DL-7, MP-H1, DL-4, and DL-5 (Figs. 4 and 6). The transgressive lag at its base is 18 to 25 cm thick and consists of angular to subangular pebbles and cobbles derived from the Archean basement. High-energy sandy fluvial to shoreline deposits (F1) that overlie this lag typify the TST. These moderately sorted pebbly, arkosic arenites to well-sorted quartz arenite beds commonly have wave-rippled tops and represent deposition on a sandy shoreface. Shale partings between some beds are interpreted to record tidal deposition of slack water fines during spring-neap flow fluctuation ([Reineck, 1972](#)). Tidal channels filled with cross-stratified sandstone and pebble lags incise shoreface deposits in areas that had a strong tidal influence.

Along low-energy segments of the shoreline and in protected bays, tidal flat sediments (F2) accumulated. These ripple cross-laminated, flaser- and lenticular-bedded quartz sandstones also contain

Table 1
Facies description and interpretation.

Facies	Sedimentary structures	Petrography	Interpretation
F1 Thickly bedded quartz arenite	Well -sorted normally graded beds; bed thickness is 10–45 cm; beds separated by 0.3–1 cm shale partings or dissolution seams; small symmetrical ripples at tops of beds; mudstone rip-ups and rounded pebbles at bed tops; less common reactivation surfaces	White to light tan; 75–90% fine to very coarse-grained rounded to subrounded quartz grains; 5–15% plagioclase and potassium feldspar; <5% blocky ankerite and microcrystalline siderite; rare sericite and chlorite; trace pristine phosphorite and fine to silt-sized reworked phosphorite; rare pyrite grains	Moderate to high-energy tidally influenced shoreline deposits and tidal channel lags
F2 Flaser and lenticular-bedded quartz sandstone	Well -sorted beds; average bedding thickness is 1 cm; ripple crossbedding; flaser bedding; mudstone rip-ups near base of beds; uncommon wavy and lenticular bedding; herringbone cross-stratification; mudstone beds contain discontinuous rippled sandstone lens and irregular carbon dissolution seams	Light tan to grey; arenaceous beds are very fine to medium-grained; 60–70% subrounded quartz; 5–15% silt-sized to fine-grained potassium feldspar and plagioclase; 10–20% Fe-carbonate; 5% microcrystalline quartz, 5–20% silt to clay sized sericite and chlorite; <5% blocky ankerite and microcrystalline siderite; mudstone beds contain 5–20% silt-sized quartz and rare muscovite	Low to moderate energy intertidal mud flats and deposits within protected bays
F3 Graded thickly bedded sandstone	Poorly sorted graded beds; average bed thickness is 50 cm; low angle ripples, planar crossbedding and trough-cross bedding at the bed tops; common mudclasts, convolute bedding, mudstone rip-ups	Light to dark grey; very fine to medium-grained quartz sandstone; 50–70% quartz; 10–40% sericite and chlorite; 5% silt-sized pyrite grains; minor silt-sized plagioclase; trace muscovite; trace 1–3 mm subhedral pyrite grains	High density turbidites on advancing delta fronts
F4 Structureless siltstone	Structureless beds; average bedding thickness is 30 cm; wavy and parallel bedding surfaces; common mud-rip ups	Light grey; 70–80% angular to subrounded silt-sized quartz grains; 20% clay sized sericite, muscovite, microcrystalline quartz grains, and dark carbon-rich muds; 10% silt-sized plagioclase grains; and minor feldspars; trace silt-sized pyrite grains	High density turbidites on delta to prodelta
F5 Organic-rich siltstone	Structureless or parallel thin laminae; common pyrite laminae	Dark grey to black siltstone; 75–80% siltstone with 8% organic material; <10–30% pyrite crystals; 5–15% disseminated angular silt sized quartz grains; 0–5% microcrystalline carbonate; disseminated pyrite crystals	Suspension deposition of fine-grained terrigenous clastics and phytoplankton
F6 Thinly bedded silty sandstone	Well -sorted, poorly graded beds; bed thickness is 2–5 cm; bedding contacts are sharp; small ball and pillow structures; uncommon ripples and low angle cross bedding	Light grey to tan; 80% rounded to subrounded quartz, silt to medium-grained; 20% clays, sericite, chlorite, muscovite; minor microcrystalline quartz grains; trace silt-sized pyrite grains	Mids shelf tempestites
F7 Desiccation cracked, wavy layered, carbonate and chert	Wavy interbedded carbonate and chert beds; Beds are 0.2–20 cm thick; common interbedded, 2 cm thick, wavy siltstone beds; common crinkled laminae; common pressure-dissolution seams; uncommon mudstone filled fenestrae; rare desiccation cracks; rare laminae and fine to medium-grained reworked phosphorite	Light grey to white; 35–50% microcrystalline chert; 35–50% fine blocky ankerite; 15% subrounded siltstone grains; trace pyrite, carbon, chlorite, muscovite; trace pristine and reworked phosphorite	Evaporation driven precipitation of chert and carbonate in intertidal to supratidal flats
F8 Chert breccia	Poorly sorted chert breccia, carbonate, and siltstone rip-ups; beds 2–20 cm thick; erosional bases; uncommon pebbles with ankerite and hematitic concentric rims; reworked crusts of francolite and hematite; francolite grains	White to light red; 20–40% chert; 20–30% coarse-grained sand to cobble-sized chert and ankerite clasts; 15–30% blocky ankerite; <10% recrystallized carbonate; 10–20% quartz siltstone and silt sized muscovite, chert and carbonate; uncommon pristine phosphorite laminae and reworked angular to rounded phosphorite clasts; 20–50% subhedral to anhedral silt sizes pyrite grains	Storm reworking of autobrecciated cherts
F9 Parallel bedded chert	Planar chert beds; average bed thickness is 4 cm; sharp bases and tops; jig saw puzzle like fitted fabric	80% white, light grey to green, and reddish grey chert; 20% very fine-grained sandstone and mudstone beds	Deep quite water precipitation of chert

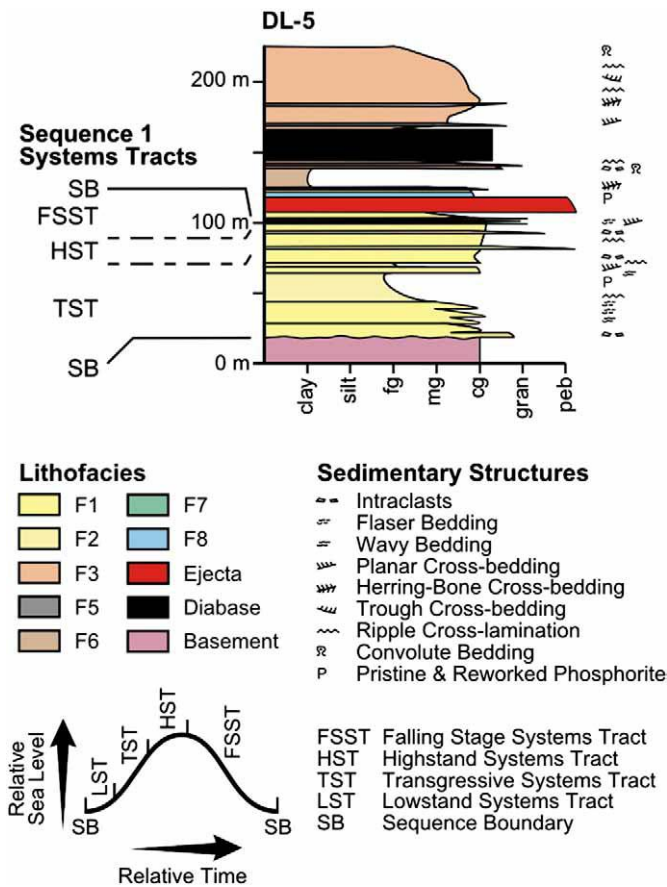


Fig. 4. Stratigraphy of sequence 1. Lithofacies are those described in Table 1. Systems tracts were interpreted using criteria established by Plint and Nummedal (2000). Lowstand deposits of sequence 1 are not present in the Baraga Basin.

discontinuous rippled sandstone lenses interpreted to record elevated flow during spring tide conditions (Reineck, 1972).

5.1.2. Highstand systems tract

The highstand systems tract (HST) ranges in thickness from 4 to 18 m and is preserved in drill cores SI-46, A-1, DL-7, DNR-MTU, MP-H1, DL-4, and DL-5 (Figs. 4 and 6). Its base is a maximum flooding surface marked by firmground development in slightly muddier shoreface sediments. Coarse sandstone beds resting on this surface are interpreted to record shoreline progradation during the apex of the highstand. These beds become more abundant through time in the HST and grade into shallower shoreface (F1) and tidal flat (F2) deposits.

5.1.3. Falling stage systems tract

The falling stage systems tract (FSST) is 5 to 9 m thick and occurs only within cores A-1, MP-H1, and DL-5 (Figs. 4 and 6). Drill cores that lack the FSST are interpreted to penetrate paleotopographic highs where the FSST was eroded or not deposited. The base of the FSST is a regressive surface of marine erosion produced through wave scouring of highstand shoreface sediments (F1) during regression. Depending on the location, the rest of the FSST is either formed of high-energy sandy (F1) or low-energy muddy (F2) shoreline deposits that are incised by tidal channels.

5.2. Sequence 2

The second sequence is up to 973 m thick and reflects the complete flooding of the Nuna margin (Figs. 5 and 6). Its base is a subaerial unconformity developed either on top of sequence 1 or the

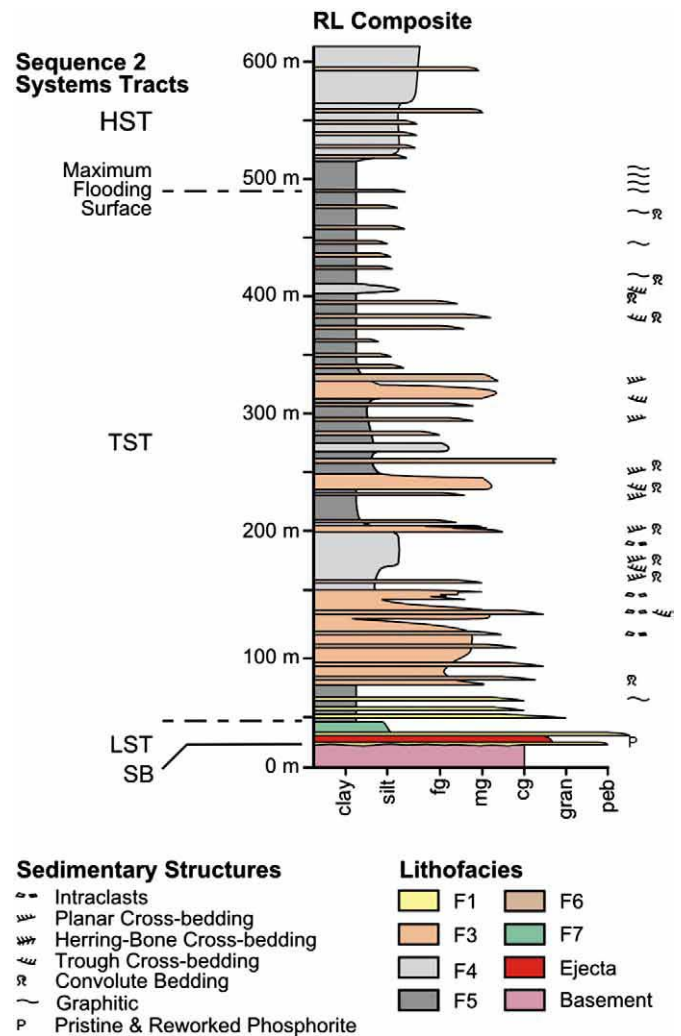


Fig. 5. Stratigraphy of sequence 2. Lithofacies are those described in Table 1. Systems tracts were erected using the criteria of Plint and Nummedal (2000) depicted on the relative sea level curve in Fig. 4.

Archean basement. Resting on this surface is peritidal chert and carbonate (F7 and F8) of the Bijiki Iron Formation. This lowstand evaporite is overlain by tidal sediments (F1 and F2) that grade into transgressive hemipelagites (F5 and F6). These silty sandstones form the upper Michigamme Formation and are interpreted to record a combination of suspension settling and storm deposition on the middle shelf. The highstand systems tract is composed primarily of progradational delta deposits (F3 and F4). Paleocurrents from cross-stratified sandstones within oriented drill core suggest that deltas were fed from the north with sediment derived from the Superior Province. Organic-rich hemipelagites (F5 and F6) and deep-water iron formation (F9) accumulated in middle shelf areas that were starved of terrigenous clastics. The falling stage systems tract is completely eroded away and is thus not preserved.

5.2.1. Lowstand systems tract

The LST varies in thickness from 3 to 28 m and is present in drill cores SI-46, A-1, RL, DL-7, DL-4, MP-H1, and DL-5 (Figs. 5 and 6). It is characterized by laminated chert and ankerite (F7) interpreted to have precipitated in supratidal ponds. Common are desiccated, subaerial exposure surfaces, stromatolites, and ubiquitous fenestral pores, which typify many Phanerozoic peritidal carbonates deposited in semi-arid settings (Pratt et al., 1992). Such evidence for periodic drying and desiccation suggests that chert and ankerite precipitated through the

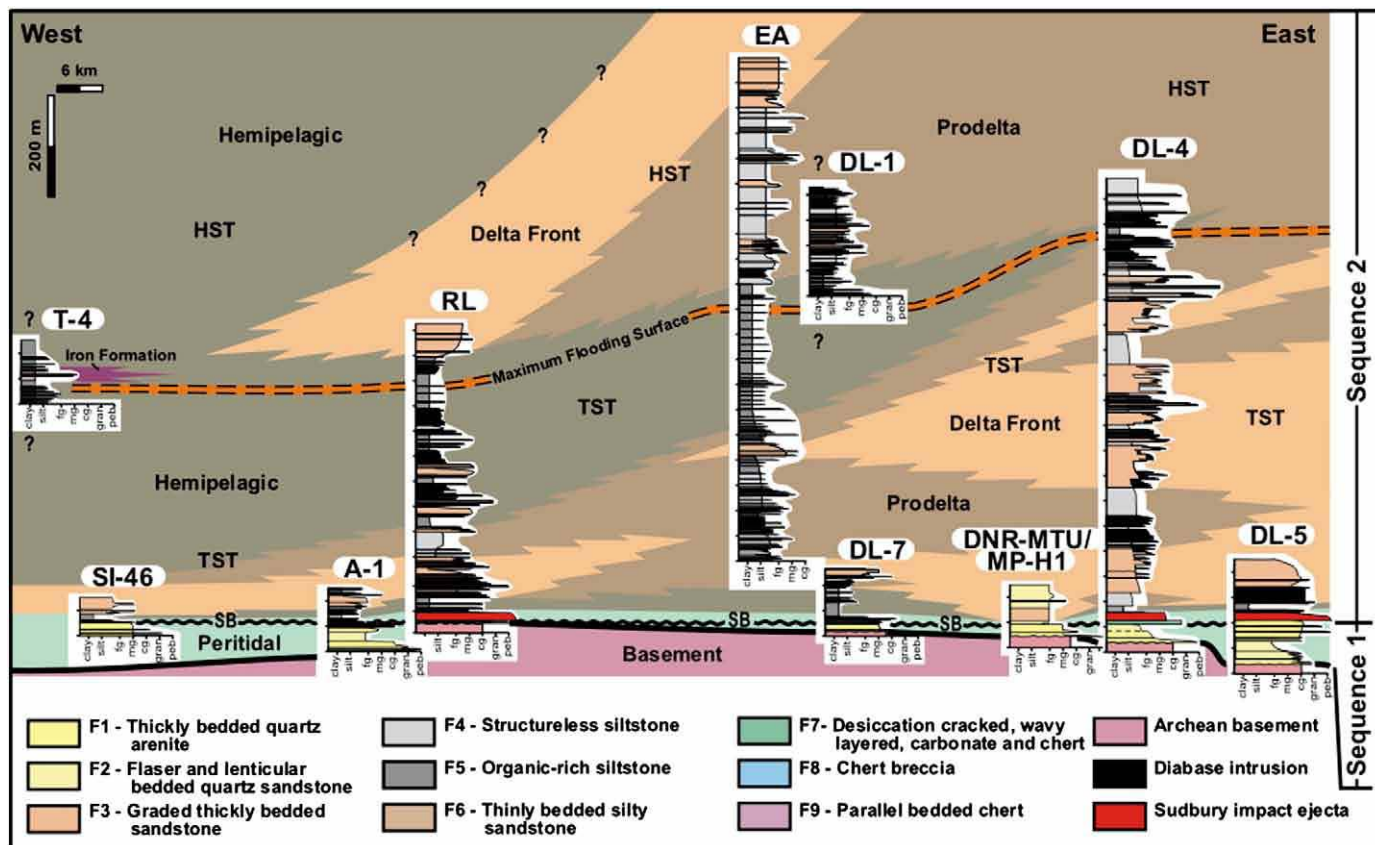


Fig. 6. Sequence stratigraphic interpretation of the Baraga Group in the study area. The Sudbury ejecta horizon is the stratigraphic datum. Lithofacies are those described in Table 1. Drill core locations are shown in Fig. 1B.

evaporitic concentration of ponded seawater (Maliva et al., 2005). Intercalated chert breccia beds (F8) record storm reworking.

These evaporites grade into terrigenous clastic tidal flat and shallow subtidal deposits (F2) that contain the Sudbury impact horizon. The catastrophic deposition of ejecta and the ensuing tsunami wave train infilled topographic lows, causing rapid aggradation and the development of an expansive peritidal environment along the coast (Pufahl et al., 2007).

5.2.2. Transgressive systems tract

The TST occurs in all drill cores and ranges in thickness from 29 to 783 m. Its base is a transgressive ravinement surface formed of pebble-sized, mud-rip ups derived from the underlying LST (Figs. 5 and 6). TST sediments consist primarily of laminated organic-rich siltstone (F5) and thinly bedded, silty sandstone (F6). The organic-rich siltstone (F5) is interpreted to be the result of suspension rain of phytoplankton debris and terrigenous clastic silt. Silty sandstone beds (F6) are interpreted to record storm deposition below fair weather wave base. Normal grading, the presence of current ripples, and erosive bottom contacts in many silty sandstone beds are typical features of distal tempestites (Seilacher and Aigner, 1991).

In the eastern Baraga Basin, deltas prograded across the middle shelf to produce decameter-scale, coarsening-upward successions (Fig. 6). Successions coarsen from prodelta siltstones (F4) to thickly bedded turbidites (F3) deposited on the advancing delta front. The retrogradational stacking pattern of such successions (Fig. 6) is interpreted to record shoreline retreat during transgression.

Along regions of the coastline that were starved of diluting terrigenous clastics, iron formation (F9) accumulated (Fig. 6). This iron formation differs from the iron carbonate-rich chert of the LST because it is formed entirely of laminated chert and lacks shallow-water sedimentary structures. Individual laminae are interpreted to record the

suspension rain of silica gel produced through discrete precipitation events in the water column. The accumulation of such chert in detritally starved, middle and distal shelf environments was likely enhanced through the suspension rain of freshly precipitated Fe-(oxyhydr)oxides, which scavenged dissolved silica from the water column and exported it to the seafloor (Fischer and Knoll, 2009; Pufahl, in press).

When present, the Sudbury impact horizon occurs at or near the bottom of the TST, where it crosscuts the basal ravinement surface and other diachronous facies boundaries (Fig. 6). Its accumulation in such proximal offshore areas caused rapid aggradation above fairweather wave base, producing a second wave-scoured ravinement surface.

5.2.3. Highstand systems tract

The preserved HST is 105 to 472 m thick and composed primarily of deltaic sediments (F4 and F5; Figs. 5 and 6). Its base is marked by a regionally persistent, 60 to 80 cm thick package of pyritic, organic-rich mudstone (F5) interpreted as the maximum flooding surface (Fig. 6). Above this interval is ~20 m of distal tempestites (F6) that are in turn overlain by at least 400 m of deltaic sediments (F3 and F4). The progradational stacking pattern of these delta deposits records the filling of available accommodation space during relative sea-level fall. As in the TST, hemipelagites (F5) and iron formation (F9) accumulated outboard of advancing deltas.

6. Baraga Group phosphorite

Sedimentary apatite was identified only in shallow-water lithofacies of the Baraga Group (cores DNR-MTU, DL-4, DL-5, and RL; Fig. 7). X-ray diffraction analysis confirms that, although not abundant, such facies contain francolite ($\text{Ca}_{10-a-b}\text{Na}_a\text{Mg}_b(\text{PO}_4)_{6-x}(\text{CO}_3)_x-y-z(\text{CO}_3\text{F})_y(\text{SO}_4)_z\text{F}_2$), which is a highly substituted carbonate fluorapatite (e.g. Nathan, 1984). Francolite is the primary phosphatic

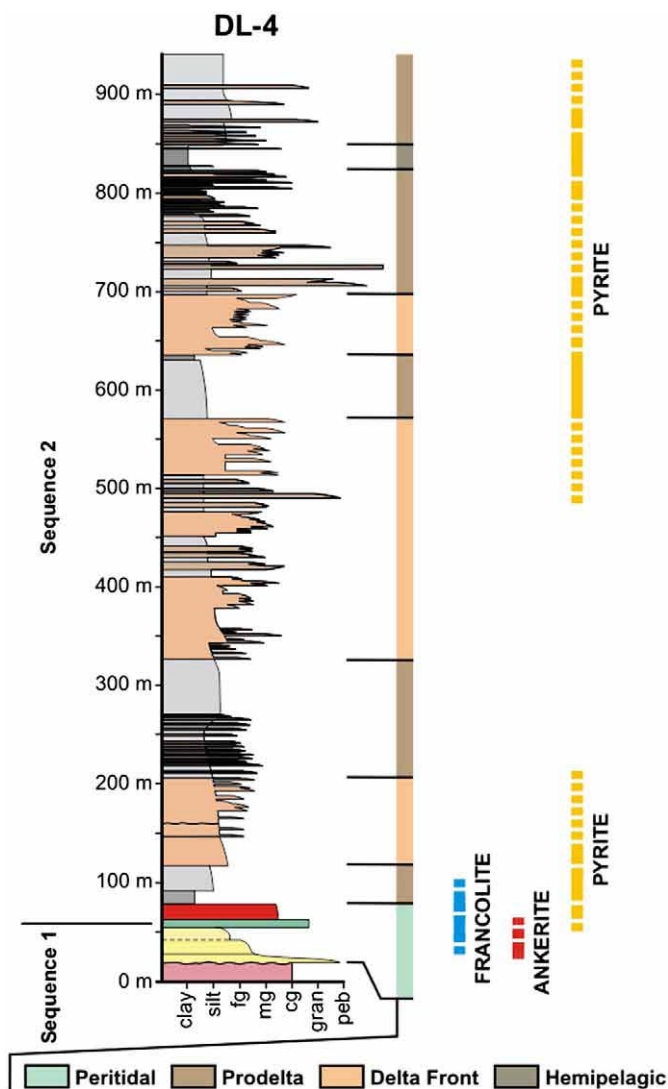


Fig. 7. Stratigraphic distribution of authigenic minerals. Lithofacies colour is keyed to the legend in Figs. 4–6.

mineral forming Phanerozoic phosphorite deposits. As in Phanerozoic analogs, francolite in the Baraga Group occurs as both pristine and reworked phosphorite (Föllmi et al., 1991). Pristine phosphorite reflects *in situ* francolite precipitation without significant reworking or winnowing, whereas reworked phosphorite is a granular deposit created by hydrodynamic processes.

Phosphorite in sequence 1 is restricted to the TST where it cements intertidal sandstones (F2) that can contain reworked francolite grains. In sequence 2, pristine phosphorite primarily occurs in stromatolitic peritidal chert and carbonate (F7) of the LST as crusts on subaerial exposure surfaces. Reworked phosphorite also occurs in the LST as discrete francolite grains within tidally deposited sandstones (F2). The exclusivity of phosphorite in shallow-water settings (Fig. 7) contrasts to many Phanerozoic depositional systems, which are phosphatic across the entire spectrum of shelf environments. Another important difference is the relatively low amount of francolite in even the most phosphatic lithofacies of the Baraga Group; francolite-rich horizons are rarely more than one cm thick.

6.1. Pristine phosphorite

Pristine phosphatic cement within tidally deposited flaser and lenticular-bedded sandstones (F2) is a honey-brown collophane

(Fig. 8A). Although not as abundant as chert and iron carbonate cements, it is volumetrically important in some laminae.

Pristine phosphatic crusts that coat subaerial exposure surfaces (F7) range in thickness from 2 to 7 mm (Fig. 8B). Each crust consists of several ~0.5 mm thick, organic carbon-rich, francolite laminae (Fig. 8C) that are interbedded to varying degrees with ripple cross-bedded sandstone lenses and stromatolites (Fig. 8D). Under plane-polarized light francolite laminae are light honey-brown in colour and contain silt-sized quartz and plagioclase grains. Ripple cross-bedded lenses are composed of fine-grained quartz and plagioclase grains with rounded, silt-sized francolite intraclasts.

Phosphatic cements are interpreted to have precipitated authigenically in peritidal environments where pore water became supersaturated with respect to dissolved phosphate. Francolite crusts formed when subaerial exposure surfaces developed in supratidal environments were flooded by minor transgressive pulses. Each crust records multiple episodes of phosphogenesis between periods of sediment reworking. The presence of interbedded sandy lenses that contain francolite rip-up intraclasts suggest tide- and storm-generated traction currents intermittently reworked pristine francolite laminae (Fig. 8E).

6.2. Reworked phosphorite

Reworked, granular phosphorite is more common in the Baraga Group than pristine phosphorite. It occurs within flaser and lenticular-bedded sandstone (F2) as discrete, silt- to fine sand-sized francolite intraclasts (Fig. 8E). Larger, pebble-sized intraclasts occur at the base of the thickest sandstone beds. Francolite intraclasts are generally well-rounded and light tan to dark honey-brown in colour. Chamositic and coated phosphatic grains also occur within some sandstone beds. Coated grains have cortices composed of numerous francolite layers that are erosively truncated by microunconformities (Fig. 8F).

Phosphatic intraclasts are interpreted as being derived from supratidal, phosphatic crusts through storm and tide-generated erosion and transport. In stark contrast to Phanerozoic phosphogenic environments, the presence of pristine francolite cement and coated grains in flaser and lenticular-bedded sandstones suggests that phosphogenesis extended into intertidal and shallow subtidal environments. Coated grains are interpreted to have formed through multiple episodes of phosphogenesis, exhumation, reworking, and burial back into the zone of phosphogenesis (Pufahl and Grimm, 2003). The presence of chamosite, an authigenic clay containing both ferrous and ferric Fe, indicates that phosphogenesis occurred beneath a suboxic seafloor (Pufahl and Grimm, 2003).

7. Iron minerals and Animikie Basin paleoceanography

Other authigenic and diagenetic minerals in the Baraga Group include siderite, ankerite, quartz, and pyrite. Changes in the abundances of these minerals (Fig. 7) record differences in the saturation and/or redox state of bottom and pore waters across the shelf, and indicate that reduced iron was readily available. Such information provides insight into how seawater was stratified in the Animikie Basin.

7.1. Ankerite and siderite

Ankerite and siderite are limited to the base of the Baraga Group. Ankerite cements tidally deposited sandstones (F1 and F2) of sequence 1 and occurs as thin laminae within evaporitic chert (F7) that forms the LST of sequence 2. Ankerite is generally microcrystalline, but can also be a coarse, blocky cement in some sandstone beds (Fig. 9A). Siderite is much less abundant than ankerite and occurs only in sequence 1 as microcrystalline cement (Fig. 9B).

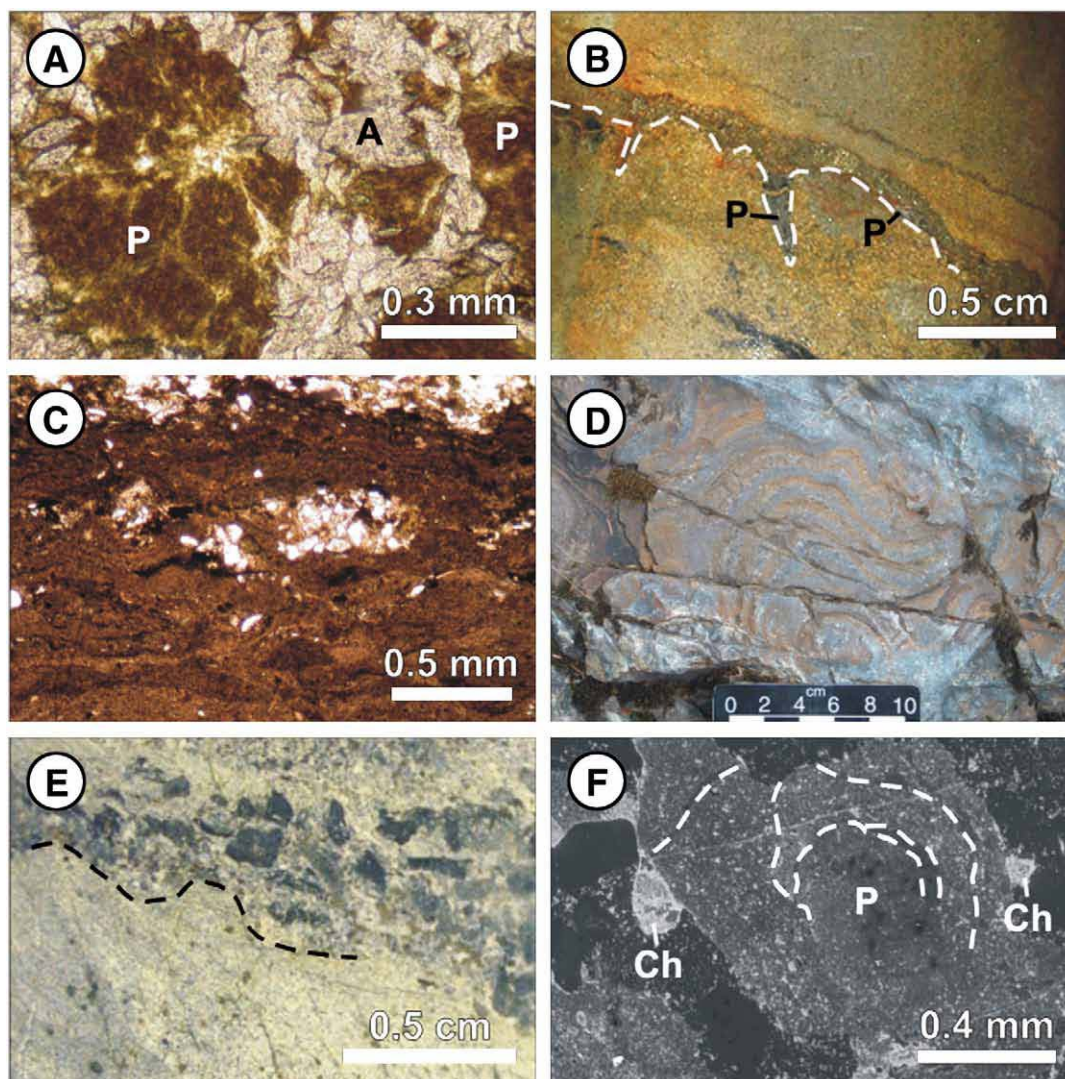


Fig. 8. Pristine and reworked phosphorite. A) Francolite (P) and ankerite (A) cement in intertidal sandstone (Facies F2) of sequence 1. B) Subaerial exposure surface (dashed line) in peritidal carbonate (Facies F7) of sequence 2. Francolite crusts (P) coat this surface and occlude desiccation cracks. Thin, grey laminae of reworked, francolite intraclasts drape the exposure surface. C) Transmitted light photomicrograph of phosphatic crust in Facies F7. Plane-polarized light. D) Stromatolitic peritidal carbonate (Facies F7) associated with phosphorite. E) Reworked, granular phosphorite laminae along subaerial exposure surface (dashed line; Facies F7) of sequence 2. Subangular phosphatic intraclasts are grey. F) Secondary electron image of chamositic (Ch) and coated francolite grain (P) in flaser and lenticular-bedded sandstone (Facies F2) of sequence 2. Cortical layers (dashed line) are erosionally truncated forming UB phosphate grains of Pufahl and Grimm (2003).

The restricted occurrence of fine-grained, Fe-carbonate cement to sequence 1, below the evaporitic lowstand deposits of sequence 2, suggests that original carbonate precipitation was related to evaporation and production of brines that infiltrated the underlying sandstones. Such seepage reflux (Adams and Rhodes, 1960; Mackenzie, 1981) produces microcrystalline dolomite in Phanerozoic evaporitic settings (Mackenzie, 1981; Dawans and Swart, 1988). Palaeoproterozoic evaporative settings likely produced iron-rich dolomite and ankerite which were later diagenetically overprinted. Their stratigraphic distribution in the Baraga Group and their textural similarity to Phanerozoic examples, point to an original seepage reflux origin. Like analogous Cenozoic dolomite formed in evaporative brines, these microcrystalline Fe-carbonate cements also crosscut lithofacies boundaries and cement overgrowths that predate compaction (cf. Choquette and Hiatt, 2008).

The coarse, blocky ankerite cement present in some sandstone beds is interpreted as having formed during burial diagenesis to greenschist facies metamorphism. It is similar to coarsely-crystalline burial cements in many altered limestones of the Phanerozoic. Burial diagenesis of organic matter-rich rocks in the Palaeoproterozoic

would have resulted in abundant reduced iron available for diagenetic carbonate phases (e.g. Ohmoto et al., 2004).

7.3. Pyrite

Pyrite occurs mainly in laminated organic-rich shales and siltstones (F5 and F6) as recrystallized framboids (Fig. 9C) and is not present in facies with abundant iron carbonates. The lack of discrete pyrite layers indicates precipitation in the water column was rare, suggesting that disseminated framboids formed within the sediment through the conversion of authigenic iron monosulfides produced during bacterial sulfate reduction (Schieber, 2002). Coarsely-crystalline subhedral to euhedral hydrothermal pyrite is also present, but is limited to fractured and faulted intervals.

Framboidal pyrite gradually increases in abundance through the LST and TST of sequence 2 (Figs. 7 and 9C). Its highest concentration in the Baraga Group occurs within these organic-rich hemipelagites. Framboidal pyrite is much less abundant in prodelta siltstones (F4) and is absent in delta front deposits (F3) of the TST and HST. Such a marked difference in pyrite abundance between hemipelagites and

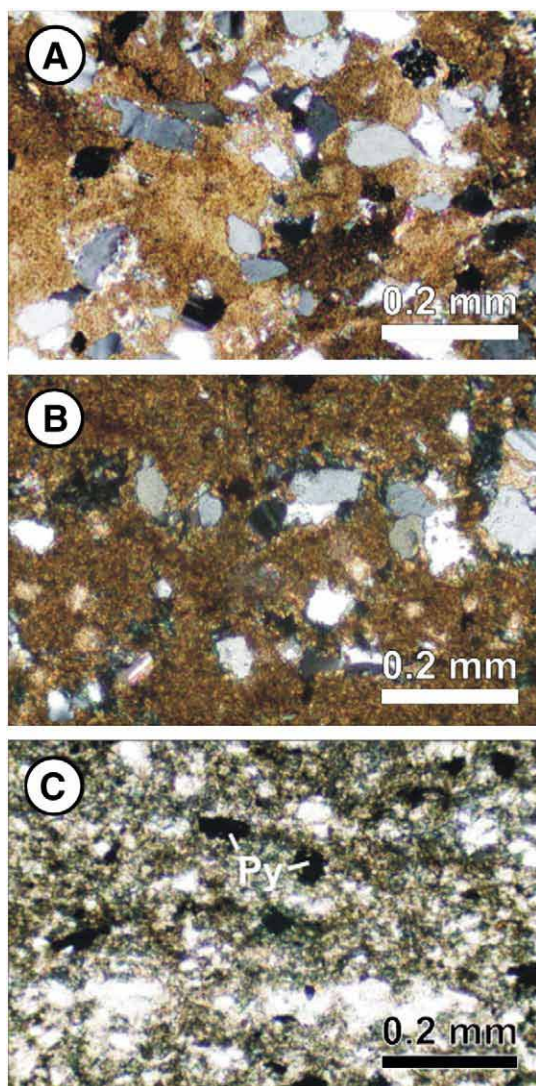


Fig. 9. Authigenic and diagenetic Fe minerals. A) Transmitted light photomicrograph in cross-polarized light of blocky ankerite cement in tidally deposited sandstone (Facies F1) of sequence 2. B) Transmitted light photomicrograph in plane-polarized light of microcrystalline siderite cementing subangular flaser and lenticular-bedded sandstone (Facies F2) of sequence 1. C) Transmitted light photomicrograph in plane-polarized light of recrystallized framboidal pyrite (Py) in organic-rich siltstone of sequence 2.

deltaic deposits (Fig. 6) is interpreted to record the high terrigenous clastic sedimentation rates and influx of river water low in sulfate associated with delta lobe progradation. The abundance of iron carbonates suggests that reduced iron was not the limiting factor in pyrite formation. Low sulfate levels, however, were a major constraint on pyrite abundance throughout much of the Precambrian (e.g. Guo et al., 2009), and sulfate levels would have been extremely low in deltaic settings during the Palaeoproterozoic.

8. Phosphorus cycling, phosphogenesis and phosphorite

Phosphorite is largely a Phanerozoic phenomenon, with only a single depositional episode occurring completely within the Precambrian (Kholodov and Butuzova, 2001; Pufahl, in press). Consequently, phosphorite depositional models are based exclusively on Phanerozoic phosphatic depositional systems. Lithofacies stacking patterns in Phanerozoic deposits indicate that phosphorite is generally associated with marine transgression and extremes in the climate state of the Earth, which causes accelerated P withdrawal from the ocean into marginal seas (Föllmi et al., 1994; Soudry et al., 2004). Phosphorite

giants in the Ordovician and Miocene are interpreted to be the result of increased delivery of P to the surface ocean through invigorated coastal upwelling during glaciations (Föllmi et al., 1993; Pufahl, in press). Large phosphatic deposits in the Permian and Mesozoic are also interpreted to have formed as a consequence of ocean–climate feedback, but through pronounced warming instead (Hiatt and Budd, 2001; Pufahl et al., 2003). A greenhouse climate and an accelerated hydrological cycle apparently increased the rate of chemical weathering and delivery of P to the oceans. Giant epeiric sea phosphorites were produced when coastal upwelling developed along favourably positioned continents (Föllmi et al., 1993; Compton et al., 2000; Pufahl et al., 2003).

Phosphogenesis within upwelling environments occurs when pore water becomes supersaturated with dissolved phosphate (H_2PO_4^- , HPO_4^{2-} and PO_4^{3-} ; Burnett, 1977; Jarvis et al., 1994; Föllmi, 1996). Phosphate is produced in oxygen minimum zones where accumulating organic-rich mud is degraded through a series of microbially mediated redox reactions. In order of decreasing energy yield, these reactions include oxic respiration, denitrification, metal oxide reduction, sulfate reduction, and methanogenesis (Froelich et al., 1979). They define distinct authigenic zones that correspond to the profiles of observed pore water concentrations of O_2 , NO_3^- , Mn^{2+} , Fe^{2+} , and SO_4^{2-} (Pufahl and Grimm, 2003). Francolite precipitates just beneath the seafloor, within 15–20 cm of the sediment–water interface, in association with these microbial reactions (Jarvis et al., 1994), particularly sulfate reduction (Arning et al., 2009). Precipitation is limited deeper in the sediment by the lack of seawater-derived fluorine and the high alkalinities that develop during organic matter respiration (Glenn et al., 1994). The development of bacterial mats prevents the escape of phosphate from the sediment to the seafloor by incorporating it in their cells. Upon postmortem degradation this phosphate is released to pore water, aiding in saturation. Some sulfur-oxidizing bacteria actively release phosphate when conditions become anoxic (Schulz and Schulz, 2005). The lack of bioturbation in many “pristine” Phanerozoic phosphorites is indicative of the low oxygen conditions in which they formed.

In non-upwelling, phosphogenic environments pore water phosphate is regulated by Fe-redox pumping (Heggie et al., 1990; Fig. 10). Fe-redox pumping is a cyclic mechanism that enriches pore water phosphate levels by first transporting phosphate adsorbed onto Fe-(oxyhydr)oxides to a suboxic seafloor. During burial, dissolution of freshly deposited Fe-(oxyhydr)oxides below the suboxic–anoxic redox boundary liberates adsorbed phosphate to pore water. The escape of phosphate out of the sediment is prevented by re-adsorption of phosphate onto Fe-(oxyhydr)oxides just above this redox interface. For Fe-redox pumping to operate efficiently as a P pump requires either repeated mixing of Fe-(oxyhydr)oxide below the Fe-redox boundary through bioturbation (Jarvis et al., 1994) or a Fe-redox boundary that oscillates vertically with time in the sediment (Pufahl and Grimm, 2003).

Sedimentologic data from the Baraga Group suggests that francolite precipitation occurred via Fe-redox pumping (Fig. 10). Unlike Phanerozoic phosphorite, however, this process was restricted to nearshore environments (Fig. 10). The presence of stromatolites and chamositic grains within phosphatic facies indicates that a shallow, suboxic seafloor was a prerequisite for phosphogenesis. Chamosite is an authigenic clay that occurs as peloids, coatings, and cement in some Phanerozoic phosphorites (Pufahl and Grimm, 2003). It is closely related to glauconite, also a common authigenic clay in some phosphatic deposits, but possesses less silica (Harder, 1980). Chamosite and glauconite contain both ferric and ferrous Fe and form through the partial reduction of Fe-(oxyhydr)oxide, indicating francolite precipitation under suboxic conditions close to the Fe-redox boundary (Glenn and Arthur, 1988; Pufahl and Grimm, 2003). Once formed, pristine phosphorite is interpreted to have been reworked into granular deposits by tidal currents and episodic storms.

Such shallow-water phosphorite accumulation contrasts to many Phanerozoic phosphatic depositional systems where francolite precipitates in the full spectrum of shelf environments (Fig. 10). This

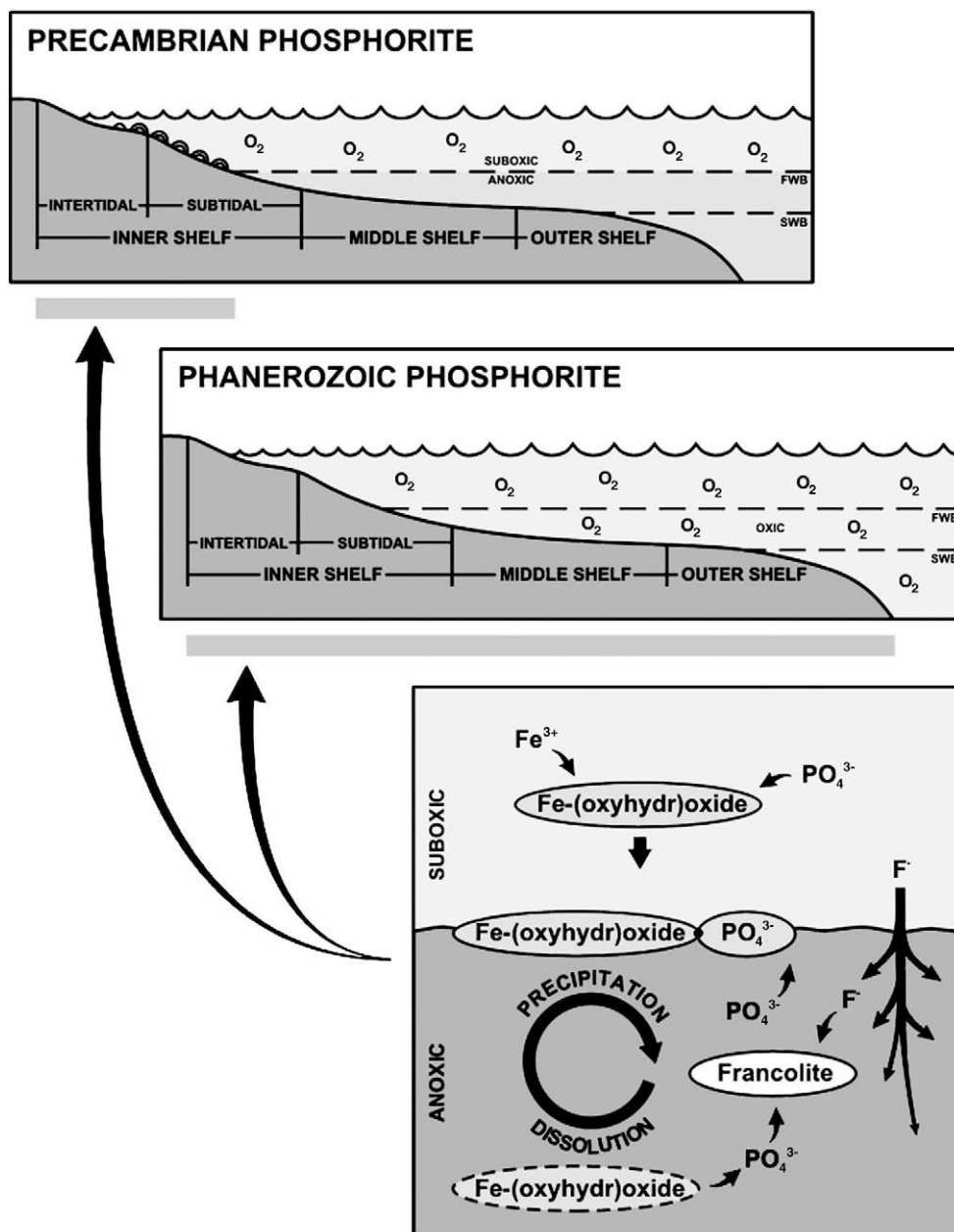


Fig. 10. Extent of phosphogenesis resulting from Fe-redox pumping on Precambrian and Phanerozoic shelves. As Fe-(oxyhydr)oxides are buried beneath the Fe-redox interface they dissolve, liberating adsorbed PO_4^{3-} to pore water. Phosphogenesis is limited in the sediment by the availability of seawater-derived F^- . The difference in the size of phosphogenic regions in the Precambrian and Phanerozoic is ascribed to the disparity in the oxygenation state of the seafloor. In the Precambrian, photosynthetic stromatolites in nearshore environments produced a suboxic seafloor that facilitated Fe-redox pumping and thus, phosphogenesis. Phosphogenesis could not occur in the middle and distal shelf because these regions were below the oxygen chemocline. This transition is interpreted to have roughly coincided with fair weather wave base. Phosphogenesis in the Phanerozoic occurs across the entire spectrum of shelf environments because the seafloor is generally well oxygenated. In this model the term “suboxic” is used as a relative measure of oxygen levels in the water column and sediment and does not refer to specific authigenic reactions or oxygen concentrations (cf. Canfield and Thamdrup, 2009). FWB = fair weather wave base; SWB = storm wave base.

difference is interpreted to reflect the dissimilarity in the oxygenation state of the seafloor, which directly affects the locus of phosphogenesis. In the Precambrian, Fe-redox pumping and thus, phosphogenesis was restricted to shallow environments where photosynthetically-produced oxygen oases impinged on the seafloor and created suboxic bottom waters. The anoxic waters that prevailed in deeper settings prohibited francolite precipitation because there was no mechanism to concentrate phosphate in the sediment. Suspension rain of Fe-(oxyhydr)oxides formed in the surface of an oxygen-stratified ocean would have released adsorbed phosphate back to the water column below the oxygen chemocline. In order for Fe-redox pumping to operate efficiently as a phosphate pump this redox boundary must

intersect the seafloor. Francolite precipitation was likely enhanced in sediment accumulating beneath a silica-undersaturated water column because the adsorption of silica onto Fe-(oxyhydr)oxides is kinetically favoured over dissolved phosphate (Konhauser et al., 2007; Fischer and Knoll, 2009).

Phanerozoic phosphorite forms across the entire shelf because the ocean bottom is generally well oxygenated, providing ideal conditions for Fe-redox pumping (Fig. 10). Fe-redox pumping is also favoured in the Phanerozoic because seawater is so severely silica-undersaturated (Calvert, 1974). Phosphogenesis in upwelling-related, oxygen minimum zones and other anoxic areas of the shelf is regulated primarily by degradation of organic matter by microbial sulfate reduction

(Arning et al., 2009). Although bacterial nitrate and metal oxide reduction also contribute phosphate to pore water, sulfate reduction releases more phosphorus during organic matter degradation (Arning et al., 2009). On the anoxic shelves of the Precambrian, however, microbial sulfate reduction was much less efficient at stimulating francolite precipitation because of the very low seawater sulfate concentrations (200 μM to 2.4 mM; Poulton et al., 2004). Such conditions likely limited the development of sulfate-reducing bacterial communities and thus, phosphogenesis.

Syndepositional phosphogenesis and reworking of pristine phosphorite by tides and storms into granular deposits during rising sea level differs from how most phosphorites in the Phanerozoic are interpreted to form. A process known as Baturin Cycling (Baturin, 1971) is often cited as a mechanism for their creation. Baturin Cycling produces pristine phosphorite during sea-level highstands when diluting terrigenous clastics are trapped in nearshore settings. Lowering of wave base during relative sea-level fall reworks pristine facies into granular deposits. Phosphorite production in the Baraga Group did not necessitate such changes in base level. Both pristine and reworked phosphorite formed in the LST and TST during relative sea-level rise. This increase in accommodation created space for phosphatic sediments to accumulate by flooding shallow areas between deltas. The precipitation and concentration of francolite was the result of combined photosynthetic oxygen production and winnowing in nearshore environments.

Some Phanerozoic phosphorites also formed through a rise in relative sea level with no intervening fall, but this process is apparently less common than Baturin Cycling. The Permian Phosphoria Formation in the western United States and the Upper Cretaceous Alhisa Formation in Jordan are interpreted to have formed through syndepositional phosphogenesis, reworking, and amalgamation of phosphatic event beds (Hiatt and Budd, 2001; Pufahl et al., 2003). A TST coupled with upwelling created detrimentally starved settings favourable for phosphogenesis; storm reworking of pristine phosphatic facies produced granular phosphorite; and amalgamation of storm-generated granular event beds formed economic phosphorite. A primary difference between these Phanerozoic phosphorites and phosphatic deposits of the Baraga Group is that bacterial sulfate reduction is interpreted to have promoted phosphogenesis in organic-rich environments across the shelf rather than Fe-redox pumping in the oxygenated nearshore.

9. The Precambrian P cycle, Baraga Group, and the sulfidic ocean model

There is only one phosphorite depositional episode that occurs completely within the Precambrian (Cook, and McElhinny, 1979; Kholodov and Butuzova, 2001; Pufahl, in press). Little is known about this interval, but it appears to span between 2.2 and 1.8 Ga, beginning in the middle of the Great Oxidation Event (ca. 2.4–2.0 Ga) just after the Huronian Glaciation (ca. 2.22 Ga), and ending during the onset of sulfidic ocean conditions (Pufahl, in press). We interpret the apparent lack of phosphorite in the Archean to reflect the anoxic chemical weathering of mafic crust that typified the early Precambrian. Such weathering would have produced little dissolved phosphate, resulting in an ocean with very low phosphate concentrations. The absence of a well-developed, oxygen-stratified ocean also probably stifled phosphogenesis because Fe-redox pumping could not operate. The very low sulfate concentrations of Archean seawater (Habicht et al., 2002; Guo et al., 2009) may have further restricted phosphogenesis by limiting the growth of sulfate-reducing bacterial communities. Without these phosphogenic processes there was no mechanism to concentrate phosphate within sediment.

We interpret the phosphatic episode in the Palaeoproterozoic to record the switch from mechanical weathering during the Huronian Glaciation to post-glacial, chemical weathering under an oxygenated

atmosphere. Oxidic chemical weathering of the young continents is interpreted to have begun ~2.4 Ga when atmospheric oxygen levels rose during the Great Oxidation Event (Holland, 2006). The Great Oxidation Event is attributed to the evolution of photosynthesizing cyanobacteria (Canfield, 2005) and a progressive loss of H_2 in volcanic gases with time (Holland, 2002). The latter is interpreted to have limited the amount of S that could combine with Fe to form pyrite, which may have also contributed to the build-up of atmospheric oxygen (Holland, 2002). After the Huronian Glaciation the oxidic weathering of granitic, post-glacial landscapes is interpreted to have increased the delivery of dissolved phosphate to the ocean. Such an increase may have been a positive feedback for further oxygen production by stimulating primary productivity (Papineau et al., 2009). Sedimentologic data from the Baraga Group suggests that the advent of a suboxic nearshore was also important because it created, for the first time, an area that could support sustained phosphogenesis. Such concentration of bioavailable P in neritic environments may have played a major role in the development of benthic microbial ecosystems and evolving eukaryotes.

The disappearance of phosphorite at ca. 1.8 Ga approximately coincides with the proposed change to a sulfidic ocean (Canfield, 1998; Anbar and Knoll, 2002; Poulton et al., 2004). The sulfidic conditions that apparently prevailed for nearly a billion years are also thought to be the result of the Great Oxidation Event (Anbar and Knoll, 2002). With the advent of oxidic weathering, sulfide minerals altered to sulfate that was delivered by rivers to the ocean where it was transformed through bacterial sulfate reduction into sulfide (Canfield, 1998; Poulton et al., 2004). By ca. 1.84 Ga the flux of sulfate was apparently sufficient to produce enough sulfide to precipitate pyrite, which titrated the ocean of dissolved Fe^{2+} and brought to an end the deposition of Superior-type iron formation (Poulton et al., 2004). The development of such widespread euxinia also likely led to the demise of phosphorite. With seawater stripped of dissolved Fe^{2+} , Fe-redox pumping and thus, phosphogenesis could not operate. Bacterial sulfate reduction was also ineffective at stimulating francolite precipitation because in euxinic seawater this phosphogenic process would have occurred in the water column and not at the sediment–water interface. Like iron formation, phosphorite did not accumulate again until the Neoproterozoic, when widespread sulfidic conditions in the global oceanic deep-water finally abated.

What is known about the Palaeoproterozoic sulfidic ocean transition is based largely on geochemical ($\delta^{34}\text{S}_{\text{pyrite}}$) and iron speciation data from Animikie Group rocks in Ontario and Minnesota (Poulton et al., 2004; Johnston et al., 2006) that are correlative to the Baraga Group (Fig. 2). The stratigraphic position of the newly discovered Sudbury ejecta horizon in Michigan, Minnesota, and Ontario (Addison et al., 2005; Pufahl et al., 2007) confirms that the deltaic and hemipelagic sedimentary rocks of the Michigamme Formation are equivalent with similar deposits of the Tyler, Rabbit Lake, Virginia, and Rove formations to the west and north. Ejecta emplacement approximately coincides with increased input of river-borne sediment to the Animikie Basin. The occurrence of minor iron formation (Fig. 6) and authigenic, Fe-carbonate cement within the Baraga Group indicates that widespread euxinia had not yet developed. Although the water column in the Animikie Basin was anoxic, it was still enriched in dissolved Fe^{2+} . These observations suggest that the change to sulfidic conditions occurred after ca. 1.84 Ga, which is the accepted age for this transition derived from the Rove Formation (Poulton et al., 2004).

10. Conclusions

1. Palaeoproterozoic sedimentary rocks of the Baraga Group were deposited in an array of environments on a tide-dominated shelf that was episodically reworked by storms. Deposition occurred through two sea-level cycles that record the inundation of the Nuna continental margin.

2. Sequence 1 (8.6–86.0 m thick) consists of a basal lag overlain by peritidal terrigenous clastics that accumulated in topographic lows along the shore of the Archean craton. Cross-bedded quartz arenite and a wavy to lenticular-bedded mudstone and siltstone dominate this sequence. During the deposition of the TST extensive tidal flats developed. Intertidal flats prograded basinward during accumulation of the HST. The FSST is characterized by tidal channels that downcut into underlying tidal sediments. Phosphorite occurs only within shallow-water environments of the TST.
3. Sequence 2 ranges in thickness from 12.0 to 973.0 m. The base of the sequence consists of peritidal chert overlain by flaser- and lenticular-bedded sandstone deposited in shallow subtidal environments. Above these sediments organic-rich hemipelagic siltstones and delta front turbidites dominate. The LST records deposition of evaporative chemical sediments in low-energy intertidal and supratidal environments. During the accumulation of the TST the rate of relative sea-level rise was greater than that of sedimentation, producing a retrogradational package of interbedded hemipelagites and delta deposits. The HST is characterized by coarsening-upward deltaic successions that record multiple episodes of lobe progradation as available accommodation space was filled. In regions between deltas where terrigenous clastic input was low iron formation accumulated. Phosphorite occurs only in shallow-water environments of the LST.
4. Phosphorite accumulation in the Baraga Group occurred only in photosynthetically-produced, nearshore oxygen oases. Phosphogenesis is interpreted to be the result of Fe-redox pumping of pore water phosphate through a suboxic seafloor. Once formed, pristine phosphorite was reworked into granular deposits by tidal currents and storms during a rising sea level. Our data suggest that Fe-redox pumping controlled phosphogenesis and the concentration of bioavailable P in benthic environments, which may apply to much of the Precambrian.
5. Syndepositional phosphogenesis and reworking of pristine phosphorite into granular phosphatic deposits during a rise in relative sea level differs from Baturin Cycling, which requires major changes in sea level to produce granular phosphorite. The proposed model does not necessitate sea level cycles, but emphasizes interplay between autogenic sedimentary processes and biologically oxygenated seawater.
6. The shallow-water phosphorite of the Baraga Group contrasts with many Phanerozoic depositional systems where phosphogenesis occurs in the full spectrum of middle and distal shelf environments. This fundamental difference is interpreted to reflect the dissimilarity in the oxygenation of the seafloor. In the Baraga Group Fe-redox pumping promoted phosphogenesis in shallow-water settings where photosynthetically-produced oxygen oases impinged on the seafloor.
7. The occurrence of iron formation and authigenic Fe-carbonate cement in neritic lithofacies implies that the transition to a sulfidic ocean postdated the deposition of the Baraga Group and correlative sedimentary rocks of the Animikie Group in Ontario and Minnesota, which has been the benchmark for understanding this oceanographic change. Our data indicate that although seawater was anoxic it was still enriched with dissolved Fe^{2+} . The change to widespread euxinia was apparently not as abrupt as previously surmised. The sulfidic conditions that eventually did prevail decoupled the Fe and P cycles and brought to an end the Earth's first phosphogenic episode. Phosphatic deposits did not form again until sulfidic conditions finally abated in the Neoproterozoic.

Acknowledgements

This paper was improved through critical review by J. Peckman and an anonymous reviewer. We are grateful to Dean Rossell, Andrew Ware, and Melanie Humphrey for thoughtful discussions while in the

field. Kennecott Eagle Mining, Cleveland Cliffs, and the Michigan Department of Environmental Quality provided access to drill core. Cole Edwards aided with sample collection; Don Osburn prepared thin sections; and Dan MacDonald assisted with the SEM. This research was supported by an Acadia University Start-up Grant and a NESRC Discovery Grant to PKP, a University of Wisconsin-Oshkosh Undergraduate Student and Faculty Collaborative Research Program Grant to EEH, and a Geological Society of America Student Research Grant to GJN.

References

- Adams, J.E., Rhodes, M.L., 1960. Dolomitization by seepage refluxion. *Bulletin of the American Association of Petroleum Geologists* 44, 1912–1920.
- Addison, W.D., Brumpton, G.R., Vallini, D.A., McNaughton, N.J., Davis, D.W., Kissin, S.A., Fralick, P.W., Hammond, A.L., 2005. Discovery of distal ejecta from the 1850 Ma Sudbury impact event. *Geology* 33, 193–196.
- Anbar, A.D., Knoll, A.H., 2002. Proterozoic ocean chemistry and evolution: a bioinorganic bridge? *Science* 297, 1137–1142.
- Arning, E.T., Birgel, D., Brunner, B., Peckmann, J., 2009. Bacterial formation of phosphatic laminites off Peru. *Geobiology* 7, 295–307.
- Baturin, G.N., 1971. Stages of phosphorite formation on the ocean floor. *Nature* 232, 61–62.
- Burnett, W.C., 1977. Geochemistry and origin of phosphorite deposits from off Peru and Chile. *Geological Society of America Bulletin* 88, 813–823.
- Calvert, S.E., 1974. Deposition and diagenesis of silica in marine sediments. *International Association of Sedimentologists. Special Publication* 1, 273–299.
- Canfield, D.E., 1998. A new model for Proterozoic ocean chemistry. *Nature* 396, 450–453.
- Canfield, D.E., 2005. The history of atmospheric oxygen: homage to Robert M. Garrels. *Annual Reviews of Earth and Planetary Science* 33, 1–36.
- Canfield, D.E., Thamdrup, B., 2009. Towards a consistent classification scheme for geochemical environments, or, why we wish the term “suboxic” would go away. *Geobiology* 7, 385–392.
- Cannon, W.F., Klasner, J.S., 1976. Phosphorite and other apatite-bearing sedimentary rocks in the Precambrian of northern Michigan. *USGS Series Circular*. 6 pp.
- Cannon, W.F., Schulz, K.J., Wright Horton Jr., J., Kring, D.A., 2009. The Sudbury impact layer in the Paleoproterozoic iron ranges of northern Michigan, USA. *Geological Society of America Bulletin*. doi:10.1130/B26517.1 published online 25 September 2009.
- Choquette, P.W., Hiatt, E.E., 2008. Shallow-burial dolomite cement: a major component of many ancient sucrosic dolomites. *Sedimentology* 55, 423–460.
- Compton, J., Mallinson, D., Glenn, C.R., Filippelli, G., Follmi, K., Shields, G., Zanin, Y., 2000. Variations in the global P cycle. In: Glenn, C.R., Prevot-Lucas, L., Lucas, J. (Eds.), *Marine Authigenesis: From Global to Microbial*. : SEPM Special Publication, 66. SEPM, Tulsa, pp. 21–33.
- Cook, P.J., McElhinny, M.W., 1979. A reevaluation of the spatial and temporal distribution of sedimentary phosphate deposits in the light of plate tectonics. *Economic Geology* 74, 315–330.
- Cook, P.J., Shergold, J.H., 1986. *Phosphate Deposits of the World: Proterozoic and Cambrian Phosphorites*. Cambridge University Press, Cambridge. 408 pp.
- Dawans, J.M., Swart, P.K., 1988. Textural and geochemical alternations in Late Cenozoic Bahamian dolomites. *Sedimentology* 35, 385–403.
- Filippelli, G.M., Delaney, M.L., 1994. The oceanic P cycle and continental weathering during the Neogene. *Paleoceanography* 9, 643–652.
- Fischer, W.W., Knoll, A.H., 2009. An iron shuttle for deepwater silica in Late Archean and early Paleoproterozoic iron formation. *Geological Society of America Bulletin* 121, 222–235.
- Föllmi, K.B., 1996. The P cycle, phosphogenesis and marine phosphate-rich deposits. *Earth Science Reviews* 40, 55–124.
- Föllmi, K.B., Garrison, R.E., Grimm, K.A., 1991. Stratification in phosphatic sediments: illustrations from the Neogene of California. In: Einsele, G., Ricken, W., Seilacher, A. (Eds.), *Cycles and Events in Stratigraphy*. Springer-Verlag, Berlin, pp. 492–507.
- Föllmi, K.B., Weissert, H., Lini, A., 1993. Nonlinearities in phosphogenesis and P-carbon coupling and their implications for global change. In: Wollast, R., Mackenzie, F.T., Chou, L. (Eds.), *Interactions of C, N, P, and S Biogeochemical Cycles and Global Change*. : NATO ASI Series. Springer-Verlag, Berlin, pp. 447–474.
- Föllmi, K.B., Weissert, H., Bisping, M., Funk, H., 1994. Phosphogenesis, carbon-isotope stratigraphy, and carbonate-platform evolution along the Lower Cretaceous northern Tethyan margin. *Geological Society of America Bulletin* 106, 729–746.
- Froelich, P.N., Klinkhammer, G.P., Bender, M.L., Luedtke, N.A., Heath, G.R., Cullen, D., Dauphin, P., Hammond, D., Hartman, B., Maynard, V., 1979. Early oxidation of organic matter in pelagic sediments of the eastern equatorial Atlantic: suboxic diagenesis. *Geochimica et Cosmochimica Acta* 43, 1075–1090.
- Glenn, C.R., Arthur, M.A., 1988. Petrology and major element geochemistry of Peru margin phosphorites and associated diagenetic minerals: authigenesis in modern organic rich sediments. *Marine Geology* 80, 231–268.
- Glenn, C.R., Föllmi, K.B., Riggs, S.R., Baturin, G.N., Grimm, K.A., Trappe, J., Abed, A.M., Galli-Oliver, C., Garrison, R.E., Ilyin, A.V., Jehl, C., Rohrlisch, V., Sadaqah, R.M.Y., Schidlowski, M., Sheldon, R.E., Siegmund, H., 1994. P and phosphorites: sedimentology and environments of formation. *Eclogae Geologicae Helveticae* 87, 747–788.
- Guo, Q., Strauss, H., Kaufman, A.J., Schroeder, S., Gutzmer, J., Wing, B., Baker, M.A., Bekker, A., Jin, Q., Kim, S.-T., Farquhar, J., 2009. Reconstructing Earth's surface

- oxidation across the Archean–Proterozoic transition. *Geology* 37, 399–402. doi:10.1130/G25423A.1.
- Habicht, K.S., Gade, H., Thamdrup, B., Berg, P., Canfield, D.E., 2002. Calibration of sulfate levels in the Archean ocean. *Science* 298, 2372–2374.
- Hall, C.R. 1985. Precambrian phosphorites of Northern Michigan. Unpublished M.Sc. thesis, Michigan Technological University, Houghton. 294 pp.
- Harder, H., 1980. Synthesis of glauconite at surface temperatures. *Clays and Clay Minerals* 28, 217–222.
- Heaman, L.M., Easton, R.M., Hart, T.R., Hollings, P., MacDonald, C.A., Smyk, M., 2007. Further refinement of the timing of Mesoproterozoic magmatism, Lake Nipigon region, Ontario. *Canadian Journal of Earth Sciences* 44, 1055–1086.
- Heggie, D.T., Skyring, G.W., O'Brien, G.W., Reimers, C., Herczeg, A., Moriarty, D.J.W., Burnett, W.C., Milnes, A.R., 1990. Organic carbon cycling and modern phosphorite formation on the East Australia continental margin: an overview. In: Notholt, A.J.G., Jarvis, I. (Eds.), *Phosphorite Research and Development*. The Geological Society of London, Oxford, pp. 87–117.
- Hemming, S.R., McLennan, S.M., Hanson, G.N., 1995. Geochemical and Nd/Pb isotopic evidence for the provenance of the Early Proterozoic Virginia Formation, Minnesota. Implications for the tectonic setting of the Animikie Basin. *Journal of Geology* 103, 147–168.
- Hiatt, E.E., Budd, D.A., 2001. Sedimentary phosphate formation in warm shallow waters: new insights into the palaeoceanography of the Permian Phosphoria Sea from analysis of phosphate oxygen isotopes. *Sedimentary Geology* 145, 119–133.
- Hoffman, P.F., 1987. Early Proterozoic foredeeps, foredeep magmatism and superio-type iron-formations of the Canadian Shield. In: Kröner, A. (Ed.), *Proterozoic Lithospheric Evolution: American Geophysical Union Series*, 17, pp. 85–98.
- Holland, H.D., 2002. Volcanic gases, black smokers, and the Great Oxidation Event. *Geochimica et Cosmochimica Acta* 66, 3811–3826.
- Holland, H.D., 2006. The oxygenation of the atmosphere and oceans. *Philosophical Transactions. Royal Society of London* 361, 903–915.
- Jarvis, I., Burnett, W.C., Nathan, Y., Almbaydin, F.S.M., Attia, A.K.M., Castro, L.N., Flicoteaux, R., Hilmy, M.E., Husain, V., Quatawnah, A.A., Serjani, A., Zanin, Y.N., 1994. Phosphorite geochemistry: state-of-the-art and environmental concerns. *Eclogae Geologicae Helveticae* 87, 643–700.
- Johnston, D.T., Poulton, S.W., Fralick, P.W., Boswell, A.W., Canfield, D.E., Farquhar, J., 2006. Evolution of the oceanic sulfur cycle at the end of the Paleoproterozoic. *Geochimica et Cosmochimica Acta* 70, 5723–5739.
- Johnston, D.T., Wolfe-Simon, F., Pearson, A., Knoll, A.H., 2009. Anoxygenic photosynthesis modulated Proterozoic oxygen and sustained Earth's middle age. *PNAS* 106, 16925–16929.
- Kholodov, V.N., Butuzova, G.Y., 2001. Problems of iron and phosphorus geochemistry in the Precambrian. *Lithology and Mineral Resources* 36, 291–302.
- Konhauser, K.O., Lalonde, S.V., Amskold, L., Holland, H.D., 2007. Was There Really an Archean Phosphate Crisis? *Science*, v 315, p. 1234.
- Mackenzie, J., 1981. Holocene dolomitization of calcium carbonate sediments from the coastal sabkhas of Abu Dhabi, U.A.E.: a stable isotope study. *Journal of Geology* 89, 185–198.
- Maliva, R.G., Knoll, A.H., Simonson, B.M., 2005. Secular change in the Precambrian silica cycle: insights from chert petrology. *Geologic Society of America Bulletin* 117, 835–845.
- Mancuso, J.J., Loughheed, M.S., Shaw, R., 1975. Carbonate–apatite in Precambrian cherty iron-formation, Baraga County, Michigan. *Economic Geology* 70, 583–856.
- Melezhik, V.A., Fallick, A.E., Hanski, E.J., Kump, L.R., Lepland, A., Prave, A.R., Strauss, H., 2005. Emergence of the aerobic biosphere during the Archean–Proterozoic transition: Challenges of future research. *GSA Today* 15, 4–11.
- Morey, G.B., Southwick, D.L., 1995. Allostratigraphic relationships of early Proterozoic iron-formations in the Lake Superior Region. *Economic Geology* 90, 1983–1993.
- Nathan, Y., 1984. The mineralogy and geochemistry of phosphorites. In: Nriagu, J.O., Moore, P.B. (Eds.), *Phosphate Minerals*. Springer-Verlag, Heidelberg, pp. 275–291.
- Nelson, G.J., 2008. Paleooceanographic constraints on Paleoproterozoic phosphorite and iron formation accumulation, Baraga Group, Michigan, USA. Unpublished M.Sc. thesis, Acadia University, Wolfville. 108 pp.
- Ohmoto, H., Watanabe, Y., Kumazawa, K., 2004. Evidence from massive siderite beds for a CO-rich atmosphere before 1.8 billion years ago. *Nature* 429, 395–399.
- Ojakangas, R.W., 1994. Sedimentology and provenance of the Early Proterozoic Michigamme Formation and Goodrich Quartzite, Northern Michigan—regional stratigraphic implications and suggested correlations. *U.S. Geological Survey Bulletin* 1904-R 31 pp.
- Ojakangas, R.W., Morey, G.B., Southwick, D.L., 2001. Paleoproterozoic basin development and sedimentation in the Lake Superior region, North America. *Sedimentary Geology* 141–142, 319–341.
- Papineau, D., Purohit, R., Goldberg, T., Pi, D., Shields, G.A., Bhu, H., Steele, A., Fogel, M.L., 2009. High primary productivity and nitrogen cycling after the phosphogenic event in the Aravalli Supergroup, India. *Precambrian Research* 171, 37–56.
- Plint, A.G., Nummedal, D., 2000. The falling stage systems tract: recognition and importance in sequence stratigraphic analysis. In: Hunt, G., Lauff, G.H. (Eds.), *Sedimentary Responses to Forced Regressions: The Geologic Society of London Special Publication*, 172, pp. 1–17.
- Poulton, S.W., Fralick, P.W., Canfield, D.E., 2004. The transition to a sulphidic ocean 1.84 billion years ago. *Nature* 431, 173–177.
- Pratt, B.R., James, N.P., Cowan, C.A., 1992. Peritidal carbonates. In: Walker, R., James, N.P. (Eds.), *Facies Models Response to Sea Level Change*. Geological Association of Canada, pp. 303–322.
- Pufahl, P.K., in press. Bioelemental sediments. In: James, N.P. and Dalrymple, R.W. (Eds.), *Facies Models 4th Edition*. Geological Association of Canada.
- Pufahl, P., Grimm, K.A., 2003. Coated phosphate grains: proxy for physical, chemical, and ecological changes in seawater. *Geology* 31, 801–804.
- Pufahl, P.K., Grimm, K.A., Abed, A.M., Sadaqah, R.M.Y., 2003. Upper Cretaceous (Campanian) phosphorites in Jordan: implications for the formation of a southern Tethyan phosphorite giant. *Sedimentary Geology* 161, 175–205.
- Pufahl, P.K., Hiatt, E.E., Stanley, C.R., Morrow, J.R., Nelson, G.J., Edwards, C.T., 2007. Physical and chemical evidence of the 1850 Ma Sudbury impact event in the Baraga Group, Michigan. *Geology* 35, 827–830.
- Reineck, H., 1972. Tidal flats. In: Kirby, J.K., Hamblin, W.K. (Eds.), *Recognition of Ancient Sedimentary Environments: Society of Economic Paleontologists and Mineralogists, Special Publication*, 16, pp. 146–159.
- Schieber, J., 2002. Sedimentary pyrite: a window into the microbial past. *Geology* 30, 531–534.
- Schneider, D.A., Bickford, M.E., Cannon, W.F., Schilz, K.J., Hamilton, M.A., 2002. Age of volcanic rocks and syndepositional iron formations, Marquette Range Supergroup: implications for the tectonic setting of Paleoproterozoic Iron Formations of the Lake Superior region. *Canadian Journal of Earth Science* 39, 999–1012.
- Schulz, H.N., Schulz, H.D., 2005. Large sulfur bacteria and the formation of phosphorite. *Science* 307, 416–418.
- Seilacher, A., Aigner, T., 1991. Storm deposition at the bed, facies, and basin scale: the geologic perspective. In: Einsele, G., Ricken, W., Seilacher, A. (Eds.), *Cycles and Events in Stratigraphy*. Springer-Verlag, Berlin, pp. 249–267.
- Soudry, D., Segal, I., Nathan, Y., Glenn, C.R., Halicz, L., Lewy, Z., VonderHaar, D.L., 2004. $^{44}\text{Ca}/^{42}\text{Ca}$ and $^{143}\text{Nd}/^{144}\text{Nd}$ isotope variations in Cretaceous–Eocene Tethyan francolites and their bearing on phosphogenesis in the southern Tethys. *Geology* 32, 389–392.
- Trow, J., 1979. Final report diamond-drilling for geological information in the middle Precambrian basins in the western portion of northern Michigan. Report UDOE OFR GJB X-1 62(79). Michigan Department of Natural Resources.
- Van Wyck, N., Johnson, C.M., 1997. Common lead, Sm–Nd, and U–Pb constraints on petrogenesis, crustal architecture and tectonic setting of the Penokean Orogen (Paleoproterozoic) in Wisconsin, USA. *Geological Society of America Bulletin* 109, 799–808.